

An Analysis of the Filter Kernel of TPIV

Andrew G. Shi* and Adam M. Steinberg†
Georgia Institute of Technology, Atlanta, GA, 30332

Tomographic particle image velocimetry (TPIV) is the de-facto standard method of measuring three-dimensional fluid velocity fields. As TPIV is based on statistical cross-correlation of particle images in finite size interrogation boxes (IB), it applies a filtering operation to any velocity variations within the IB. Subsequent analysis of TPIV data is then applied on this filtered velocity field; understanding the nature of the filtering is beneficial to such analysis. This paper identifies a filter kernel associated with TPIV. The TPIV filter is obtained by running TPIV on a procedurally-generated step-response velocity field and analyzing the gradient. In one-dimension, the profile of the filter resembles a blend between a Gaussian and "Mexican-hat" wavelet; the three-dimensional kernel is constructed by autoconvolution of the profile in the three spacial dimensions. Varying the (IB) used in the adaptive TPIV cross-correlation indicates a direct relationship between the width of the filter and the IB size. A direct numerical simulation (DNS) of a premixed flame in homogeneous isotropic turbulence is used to validate the filter. Application of the filter on both reacting and non-reacting portions of the flame demonstrates that the filter can accurately estimate the TPIV output across a wide range of IB sizes.

I. Introduction

The ability to visualize flows is essential in the research of fluids. Today, one of the primary methods used for this purpose is particle image velocimetry (PIV). Fundamentally, PIV works by measuring the displacement of tracer particles seeded into the fluid as they follow the flow dynamics. When the flow is illuminated, light is scattered by the tracer particles and captured by imaging devices. By taking multiple images over short intervals of time, the motion of the particles can be determined and then used to calculate the overall instantaneous velocity field [1]. Traditional PIV uses a single camera that images a plane of the flow, resulting in a two-dimensional, two-component velocity field. This restriction to only 2D often limits the types of analyses that can be done with traditional PIV. For applications that require a three-dimensional diagnostic, more complex PIV setups have been developed, including tomographic particle image velocimetry (TPIV). Unlike in traditional PIV setups, TPIV involves illuminating a volume, rather than a plane, of the flow and using multiple, typically at least four, cameras to capture the light scattering from various viewing angles. The simultaneous images of the volume are used in a 3D cross-correlation algorithm to reconstruct a 3D representation of the particle field (i.e. tomogram); the most commonly used algorithm is the Multiplicative Algebraic Reconstruction Technique (MART), which was chosen for the analysis herein. The 3D particle field representations are analyzed in a similar manner to traditional PIV to calculate the 3D velocity field [2].

Since its introduction by Elsinga et al. in Ref. [2], TPIV has now emerged as the de-facto tool for measuring instantaneous three-dimensional, three-component velocity fields, with applications encompassing a wide variety of flows including boundary-layer interactions [3], combustion [4], and even biological behavior [5]. Yet, despite its widespread use, little is known about how a TPIV velocity field deviates from the actual, exact velocity field as a result of performing TPIV. That is, when TPIV is used to capture the velocity field of a flow at a resolution larger than the flow's smallest velocity scales, the measured velocity field can be described as the result of a "filtering" operation imposed onto the true velocity field at a scale Δ related to the interrogation box (IB). This can be expressed mathematically as:

$$\tilde{u}_i(\mathbf{x}) = u_i(\mathbf{x}) * \mathcal{G}_{\text{PIV}}(\mathbf{x}) + n(\mathbf{x}), \quad (1)$$

where \tilde{u}_i is the measured velocity, u_i is the true velocity, \mathcal{G}_{PIV} is the filter imposed by the TPIV operation, and n represents the noise added during the measurement and TPIV cross-correlation. In this context, the TPIV filter kernel corresponds to a spatial filter of a width on the order of the final interrogation box (IB) volume over which the particle motion is convolved.

*Undergraduate Student Researcher, Daniel Guggenheim School of Aerospace Engineering, AIAA Student Member

†Associate Professor, Daniel Guggenheim School of Aerospace Engineering, AIAA Associate Fellow, adam.steinberg@gatech.edu

Having knowledge on the nature of the filter kernel of TPIV is beneficial for many applications that require further analysis of TPIV results. One such example is the study of reacting turbulence using Large Eddy Simulations (LES), described in brief as follows. The central idea of LES is to reduce the computational cost of computational fluid dynamics (CFD) modelling, as compared to direct numerical simulation (DNS), by separating the large and small scale motion of the flow and disregarding the latter; this is done via filtering of the governing equations (the Navier-Stokes equations). However, the small-scale information remains important, as LES models the influence of the unresolved subfilter scales (SFS) on the larger resolved scales. This is evidenced by the transport equation for the kinetic energy of the filtered flow, $k = \frac{1}{2}\tilde{u}_i\tilde{u}_i$, expressed as:

$$\frac{\partial k}{\partial t} + \tilde{u}_i \frac{\partial k}{\partial x_j} = -\underbrace{\frac{\tilde{u}_i}{\bar{\rho}} \frac{\partial \bar{p}}{\partial x_i}}_{\alpha_p} + \underbrace{\frac{\tilde{u}_i}{\bar{\rho}} \frac{\partial \tau_{ij}}{\partial x_j}}_{\alpha_v} - \underbrace{\frac{\tilde{u}_i}{\bar{\rho}} \frac{\partial \mathcal{T}_{ij}}{\partial x_j}}_{\alpha_{sfs}}, \quad (2)$$

where, α_p , α_v , and α_{sfs} represent the work done by the resolved pressure, resolved viscous shear, and the unresolved turbulent stresses, respectively [6]. The subfilter-scale stress tensor, $\mathcal{T}_{ij} = \bar{\rho}(\widetilde{u_i u_j} - \tilde{u}_i \tilde{u}_j)$, represents the transfer of momentum between the scales larger and smaller than the filter scale Δ ; this term is unclosed and must be modeled. Most models of SFS used in LES are based on non-reacting turbulent flows. This is despite the fact that the physics of reacting flows is distinct from classical non-reacting, incompressible flows; in turbulent premixed flames, the classical equilibrium energy cascade is influenced by the interaction of chemical and mechanical (kinetic) energies. As a result, while LES models predict a classical forward cascade behavior (energy transfer from large to small scales), recent DNS studies showed deviation from this behavior with the presence of mean backscatter (upscale energy transfer) [7–10]. Attempts to directly measure α_{sfs} are limited by the fact that the measured velocity fields must be fully resolved; clearly, this poses an inherent problem for TPIV as the filtered product of velocities in \mathcal{T}_{ij} require estimation of u_i in Eqn. (1). To get around this limitation, a fully resolved velocity field must first be estimated from the available TPIV measurements via deconvolution prior to calculation of α_{sfs} [11, 12]. In order to perform this deconvolution accurately though, the characteristics of the filter imposed by the measurement must be known; this is where the TPIV filter kernel would be applied with great utility.

The objective of the work in this paper is to present a method for estimating the filter kernel of TPIV and use said method to identify the shape and nature of the TPIV filter kernel. The validity of the filter kernel result will be evaluated by simulating a TPIV measurement using DNS velocity fields and comparing the measured velocity field with the field generated by filtering the DNS field with \mathcal{G}_{PIV} .

II. Analysis Method

The approach employed to obtain the convolution filter imposed by TPIV processing involves creating a step-response of the velocity field, as described by Elsinga and Westerweel [13]. To summarize, Elsinga and Westerweel use a direct approach to obtain the 1D point spread function (PSF) (i.e. the convolution kernel), based on the cross-correlation analysis of a synthetic PIV image containing a step change in the particle displacement field. Spatial differentiation of the measured displacement field in a direction perpendicular to the step, followed by normalization with the step height, gives the normalized pulse response, or PSF. The 3D TPIV filter kernel can then be determined using the PSF. Consequently, a single PIV image is sufficient to estimate the convolution kernel.

While the analysis performed by Elsinga and Westerweel [13] was restricted to two-dimensional PIV, the work presented herein seeks to extend the method to a three-dimensional velocity field. Figure 1 shows the general procedure used to obtain \mathcal{G}_{PIV} .

First, the TPIV algorithm must be used to produce \tilde{u}_i . A one-dimensional flow with a step in x -velocity is created as shown in Fig. 1(a); the velocity is set to $U_x = \pm 10$ m/s above and below the step, respectively. Only a single component of velocity is considered in this study. Next, a pair of particle tomograms is generated for the imposed velocity field (Fig. 1(b)). Tomograms were generated at a resolution of $512 \times 512 \times 512$ vx with 75,000 total particles over a cube with a side length of 7 mm, effectively quadrupling the number of cells of a single $x - y$ plane of DNS. The tracer particles were randomly seeded inside the first tomogram with a uniform probability distribution (equivalent to a constant gas density flow). The second tomogram contained the same particles, convected by the imposed flow using the classic Runge-Kutta (RK4) method [14]. Each particle was assigned a three-standard-deviation Gaussian intensity profile of 5 voxels wide. The time separation between two tomogram snapshots was set to 5 μs . These settings represent the recommended targets for TPIV, including average particle density of 7-10 particles per target interrogation box and an

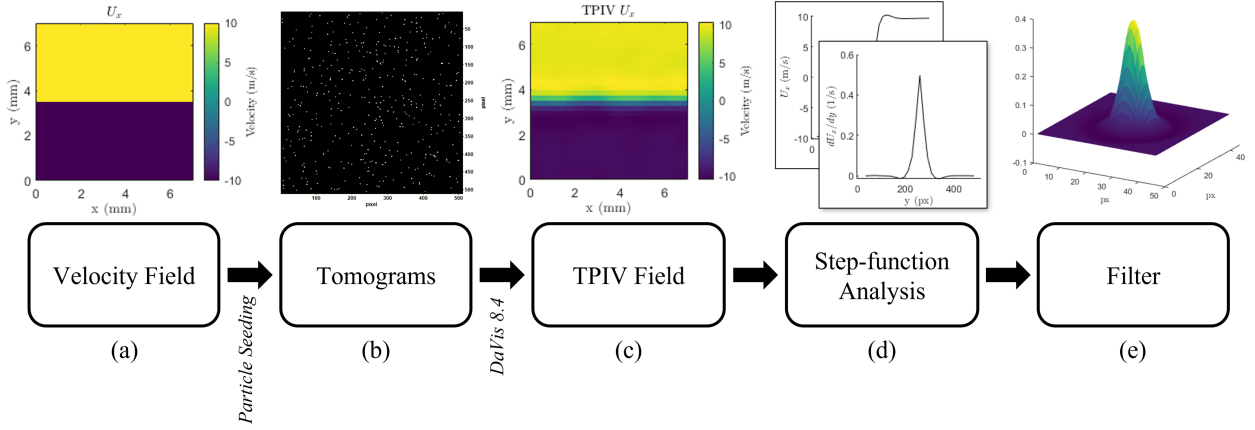


Fig. 1 A flowchart of the process to obtain the TPIV filter from an analytical velocity field.

average particle displacement distance of $1/4 - 1/3$ of the interrogation box width [1].

Processing of tomograms and calculation of TPIV velocity fields through direct cross-correlation was performed using the LaVision DaVis 8.4 software. Five different interrogation boxes were used to investigate how the filter would scale with IB size; namely 24 vx, 32 vx, 48 vx, 64 vx, and 96 vx, all with an overlap of 75%. The software's native universal outlier detection and removal algorithm was also used. The resulting TPIV velocity fields, such as the field displayed in Fig. 1(c), were averaged across the two homogeneous directions (x and z), to obtain a one-dimensional mean velocity profile across the step, as shown schematically in Fig. 1(d). Computing the gradient of the mean velocity profile yields the one-dimensional convolution kernel, which is then used to obtain the three-dimensional \mathcal{G}_{PIV} shown in Fig. 1(e).

In order to transform the one-dimensional filter profile into three-dimensions, multiple methods were considered. Initially, the 1D profile was revolved such that any given point of the kernel is a function of radial distance from the central element. The radial \mathcal{G}_{PIV} profile is then weighted by the weighing function $w(r) = r^2$ to compensate for larger number of points contained in a spherical shell of radius r , i.e. how surface area scales with radius. However, this method proved ineffective, as even with the weighting factor, it over-emphasized outer values of the filter, including over-expressing negative values of the filter. In addition, this modification of the shape of the filter does not make sense with the output of the step-response PIV field, since the weighting factor essentially "stretches" the filter shape into a narrow spike, which is not seen in the actual step-response gradient.

Instead, an "autoconvolution" method was used, where the profile acts as its own filter to extend a dimension. In other words, given a one-dimensional profile, the profile is copied and "stacked" side-by-side such that a square two-dimensional kernel is formed. Each profile is scaled by the magnitude of its location with respect to the original one-dimensional profile. For example, consider the slices of the two-dimensional filter highlighted by the red planes in Fig. 2(a). If the 1D profile is superimposed perpendicular to the planes, each plane corresponds with a different magnitude of the profile; thus, the highlighted slices are multiplied by the respective magnitudes, the result of which can be seen in Fig. 2(b). The slice at $px = 0$ has the maximum magnitude as it corresponds with the maximum location of the 1D profile, while the slice at $px = 20$ has a negative magnitude, as the 1D profile at that location is negative as well. After the 2D profile is obtained, a similar procedure is used to transform it into three-dimensions; that is, 2D profiles are stacked onto each other, with each plane being scaled by the magnitude of the 1D profile at that location. Finally, the now-cubic 3D filter kernel is normalized to a overall sum of one.

Validation of the TPIV convolution kernel was done by comparing the DNS velocity fields filtered using the three-dimensional version of \mathcal{G}_{PIV} and the same velocity field generated by DaVis 8.4. The direct numerical simulation used in this study is identical to that described by Darragh et al. [15, 16] for the Lagrangian analysis of enstrophy dynamics and analysis of particle pair dispersion in turbulent premixed flames. The authors have kindly shared the dataset for this study and the readers are referred to Ref. [15, 16] for further details of the numerical setup. The details of the DNS simulation are summarized in Table 1. To generate the TPIV fields of DNS, the same aforementioned tomogram generation process was used on the DNS velocity field.

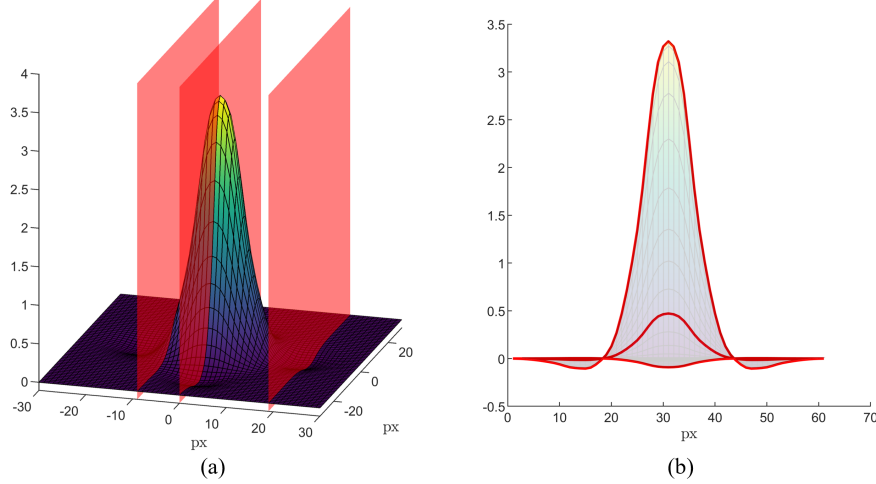


Fig. 2 Visualization of the 1D to 2D filter generation process. (a) The intensity of a 2D filter generated from a 1D profile with cross-sections highlighted in red. (b) Side-view of the 2D filter, with previously highlighted cross-sections outlined in red.

\mathcal{D}	$256 \times 256 \times 4096$	Number of cells
	$0.7 \text{ mm} \times 0.7 \text{ mm} \times 11.2 \text{ mm}$	Physical Dimensions
Δx	0.70037 cm	Cell size
ε	$1.32 \times 10^6 \text{ erg/cm}^3\text{s}$	Energy injection rate
U_δ	469.3 cm/s	Turbulent velocity at scale δ_L
U	1182 cm/s	Turbulent velocity at scale L
U_{rms}	1359 cm/s	Turbulent r.m.s. velocity
U_l	785 cm/s	Unburned integral velocity
l	$2.05 \times 10^{-1} \text{ cm}$	Integral length
η	$1.382 \times 10^{-3} \text{ cm}$	Kolmogorov length scale in reactants
τ_{ed}	$5.922 \times 10^{-4} \text{ s}$	Eddy turnover time L/U
Da	0.19	Damkohler number
Ka	142	Karlovitz number

Table 1 Physical model parameters of the highly turbulent premixed methane–air flame simulated in the present study. [15, 16]

Alternative Approaches

It should be noted that methods that utilize Fourier analysis and optimization-related techniques to obtain the convolution filter were considered and attempted but ultimately proved unsuccessful. Theoretically, the convolution theorem states that division of the Fourier transform of the PIV field by the velocity field results in the Fourier transform of the filter kernel. However, in discrete applications, a fast Fourier transform algorithm is a type of circular convolution Oppenheim and Schafer [17], which is distinct from the type of circulation used in the current application. In addition, Fourier analysis is extremely sensitive to noise and perturbations in the data; even the smallest divergence of a measured PIV value from an exact result causes extreme errors in the shape resulting filter kernel. Given that PIV is inherently non-exact and noise-prone, this renders Fourier analysis not applicable to this current context.

Regarding the optimization approach, optimization attempts were almost always highly sensitive to various processing parameters. A large portion of optimization trials resulted in filter shapes that significantly diverged from the Mexican-hat Gauss or any sensible filter shape. Even small changes in parameters such as initial condition for the optimizer, filter kernel size, and TPIV interrogation box size cause large differences in the output of the optimizer. Additionally, each

solution resulted in a relatively large convergence error, indicating that the solution may not be the most optimal; it also suggests that finding a universally appropriate TPIV filter is may be an ill-posed problem. Hence, the step-response approach was decided to be the most appropriate method for evaluation of the filter shape.

III. Results and Discussion

The mean one-dimensional TPIV velocity profile across the step and its derivative are shown in Fig. 3(a-b) for a variety of IB sizes. The mean velocity profile shows an overshoot across the step, similar to findings in Ref. [13]. Since the PIV output is at a lower resolution than the DNS input fields, values that correspond to a DNS location are interpolated into the profiles seen in Fig. 3(b), and then symmetrized to obtain the profiles in Fig. 3(c). The corresponding shape of the filter resembles a Gaussian, except with the presence of regions of negative value (e.g. at around ± 20 px for $IB = 32$ in Fig. 3(c)); since a Gaussian function is strictly positive ($G_{\text{Gaussian}} > 0 \forall x$), classifying the filter as a true Gaussian is inaccurate. Yet, the obtained shape does not oscillate for multiple periods either; starting from the peak in the center, its intensity approaches a negative minimum and then approaches zero from the negative side. A wavelet that behaves in this specific manner is that of the "Mexican hat", or Ricker, wavelet [18]; however, the valleys present in a Mexican-hat wavelet are much greater a magnitude than seen in the filter shape. Therefore, the filter shape is most accurately described as a hybrid "Mexican-hat Gauss" profile, similar to that observed and reported elsewhere [13, 19].

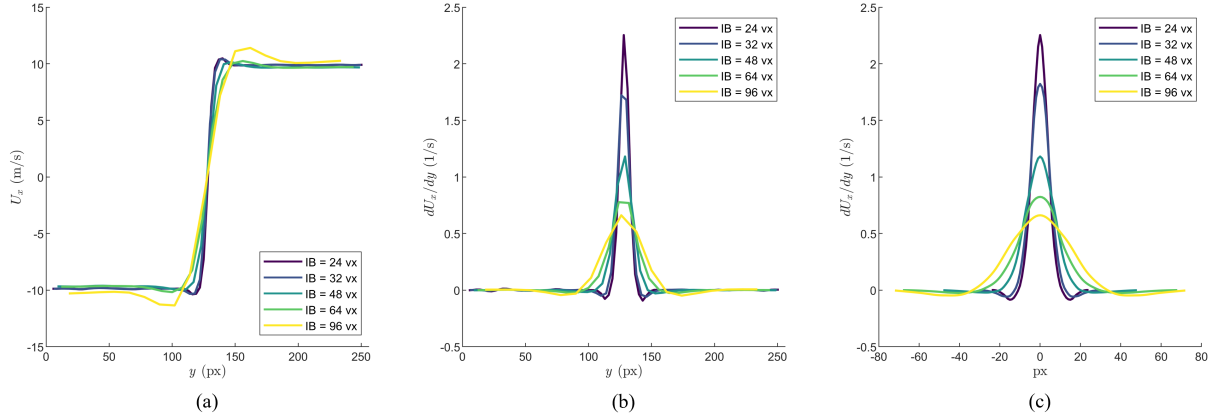


Fig. 3 One-dimensional profiles of the result from applying TPIV on the step-response velocity field. (a) The velocity profiles over a range of IB sizes. (b) The velocity gradients. (c) The velocity gradients symmetrized, interpolated, and centered over the step-change.

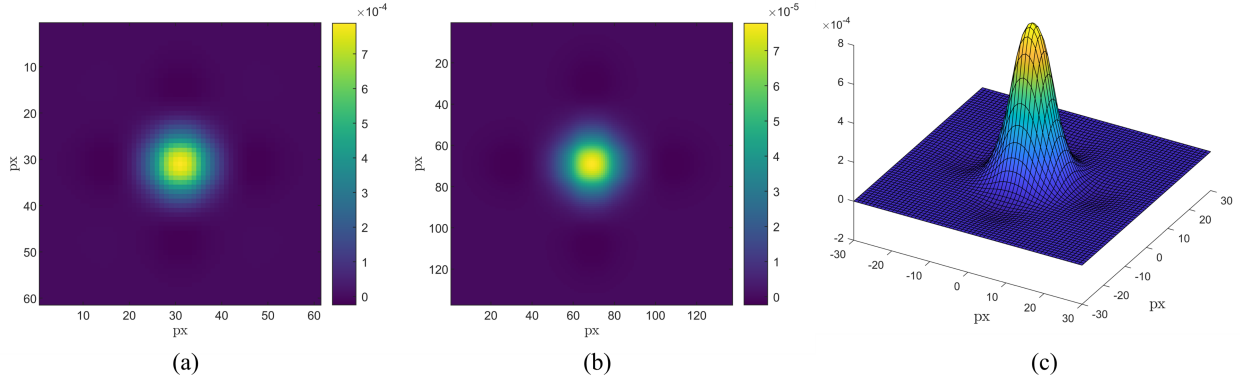


Fig. 4 Intensity visualization of the TPIV filter kernel. (a) The central slice of the filter for $IB = 32$ vx. (b) The central slice of the filter for $IB = 64$ vx. (c) A surface representation of the central slice of the filter for $IB = 32$ vx.

The one-dimensional profiles are transformed into three dimensions through the process explained above. Figure 4(a-b) shows the central 2D-slice of the filter kernels for IB = 32 vx and IB = 64 vx, respectively; normalization was applied accordingly. A surface representation of the intensity is included in Fig. 4(c). The central 1D profile of all IB sizes are plotted in Fig. 5(a). Clearly, the width of the convolution kernel increases and amplitude decreases as IB size is increased. It can also be observed that the the central portion of the filters seem to have similar sizes when plotted in the same area; for example, the IB = 32 vx filter in Fig. 4(a) has less than half the filter width as the IB = 64 vx filter in Fig. 4(b) in pixels, yet the central portions looks to be similar proportionally to each other. Indeed, this observation is confirmed once the filters are normalized by the filter width. As shown in Fig. 5(b), normalization of the filters results in virtually identical filter shapes, indicative of the fact that interrogation box size does not affect the shape of the filter; only the size of the changes, as expected, and thus the magnitudes of the filter is changed accordingly due to normalization.

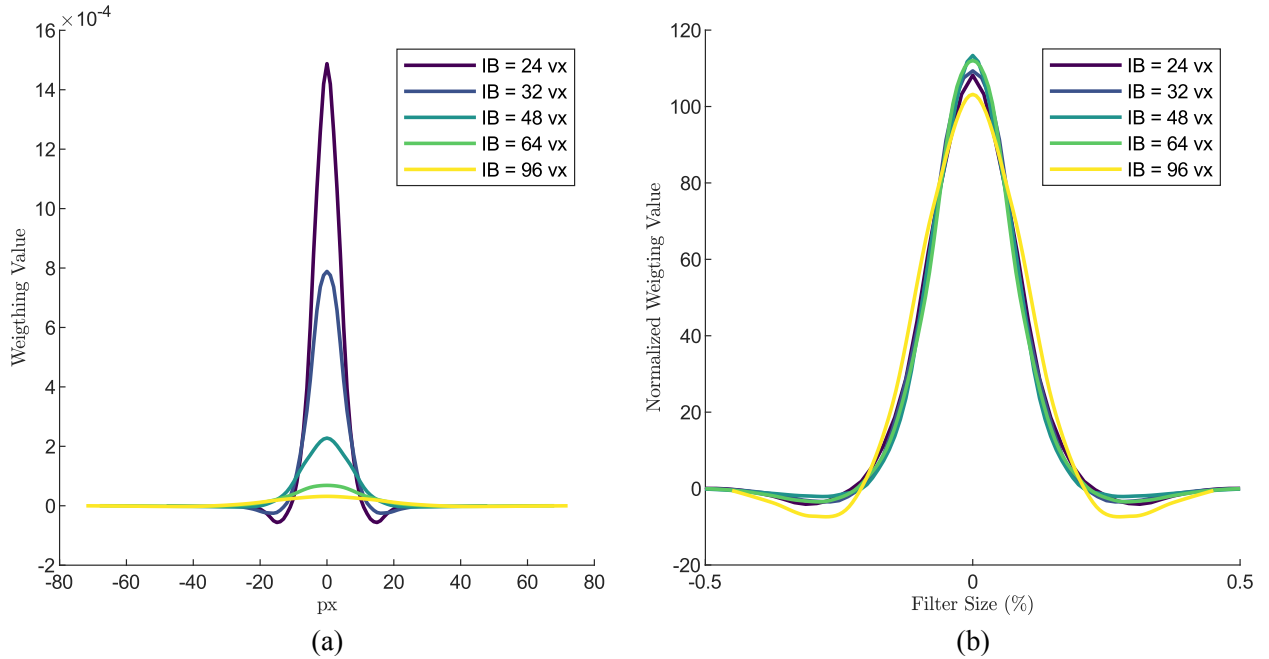


Fig. 5 (a) Central profile of the filters for all IB sizes plotted over the same axis scale. (b) Central profiles normalized by filter width.

A more quantitative description of the shape of the filter can be given in terms of a function curve-fit. Since the filter kernel can be fully described by its 1D profile, a one-variable function is sufficient to describe the shape the 3D TPIV filter. As remarked previously, the filter is characterized as a "Mexican-hat Gauss" profile, indicating the fit-function must incorporate elements of both the Gaussian function and the Mexican-hat wavelet. The Gaussian function can be represented as:

$$g(x) = \frac{a}{\sigma\sqrt{2\pi}} \exp\left(-\frac{x^2}{2\sigma^2}\right), \quad (3)$$

where a is the amplitude, σ is the standard deviation, and x is the distance away from the center of the filter. The Mexican-hat wavelet is expressed as:

$$\psi(x) = \frac{2a_M}{\sqrt{3\sigma_M\pi^{1/4}}} \left(1 - \frac{x^2}{\sigma_M^2}\right) \exp\left(-\frac{x^2}{2\sigma_M^2}\right), \quad (4)$$

where a_M and σ_M have the same meanings as in (3) but with a subscript to distinguish it from its counterparts when curve-fitting. The Mexican-hat wavelet function is derived by taking the negative normalized second derivative of (3) [18]; it is also known as the difference of Gaussians function. To represent a hybrid Mexican-hat Gauss profile, (3) and

(4) are superimposed on each other as:

$$f(x) = g(x) + \psi(x) = \frac{a}{\sigma\sqrt{2\pi}} \exp\left(-\frac{x^2}{2\sigma^2}\right) + \frac{2a_M}{\sqrt{3}\sigma_M\pi^{1/4}} \left(1 - \frac{x^2}{\sigma_M^2}\right) \exp\left(-\frac{x^2}{2\sigma_M^2}\right). \quad (5)$$

The empirical filter data is curve-fit to (5).

To allow the curve-fit function profile to be applicable to all IB sizes, the normalized profiles of the various IB sizes in Fig. 5(b) will be averaged into a singular empirical filter profile. In addition, the profile is further normalized by magnitude such that its overall sum is one. The empirical data, and the results of the curve-fit, are shown in Fig. 6, while the coefficients and relevant quantities of the resulting function are listed in Table 2. The high coefficient of determination (R^2) value indicates a very strong correlation between the curve-fit and the empirical data. Those who intend to generate a TPIV filter using the curve-fit function should (1) decide on a filter width in pixels (approximately twice that of the IB), (2) assign intensity values for each pixel location (relative to the center) based on the curve-fit function, (3) autoconvolve the 1D profile twice to create a 3D filter kernel, and (4) normalize the magnitude of the filter kernel values to an overall sum of unity.

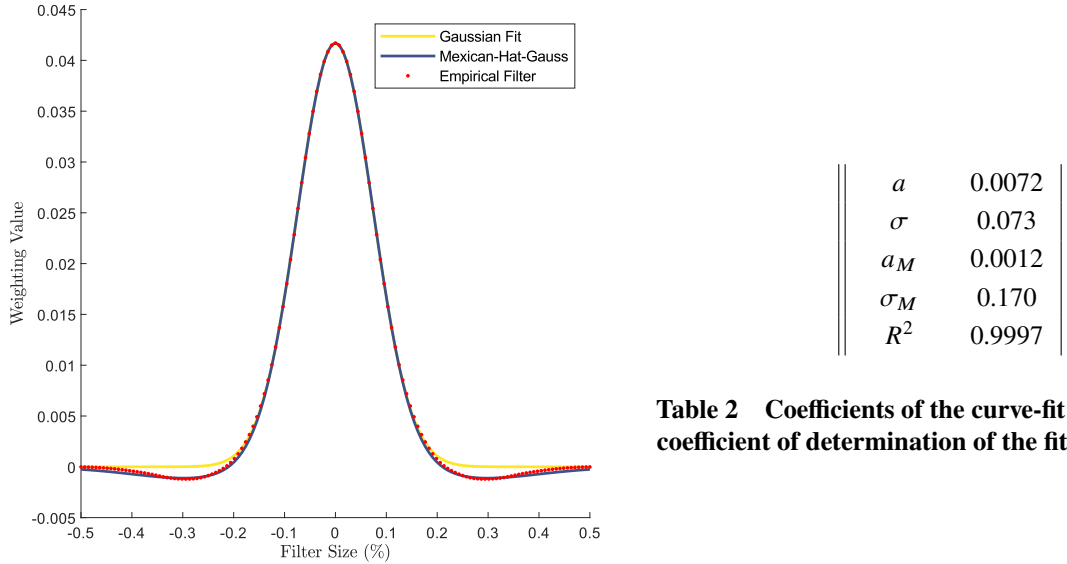


Table 2 Coefficients of the curve-fit function and the coefficient of determination of the fit.

Fig. 6 The curve-fit profile plotted over the empirical filter profile. A standard Gaussian curve-fit is also plotted for reference.

Application of the three-dimensional \mathcal{G}_{PIV} on a non-reacting portion of a fully-resolved DNS field at various IB sizes is displayed in Fig. 7; the filtered fields are compared with the corresponding TPIV field. Note that only the x -component of velocity is included for brevity; other velocity components show similar results. As is expected, the result of applying a larger filter/IB (such as IB = 64 vx and IB = 96 vx in Fig. 7(d-e)) on a fully-resolved velocity field results in removal of larger fine-scale structures than with using a smaller filter/IB (namely Fig. 7(a-b)). Visual comparison of filtered DNS with TPIV velocity reveals excellent agreement between the two datasets, including detail-smoothing and magnitude preservation.

For a more global comparison of \tilde{u}_{PIV} and $u * \mathcal{G}_{\text{PIV}}$, joint PDFs are constructed and shown in Fig. 8, along with the computed correlation coefficient. All three components of velocity are used in the comparison. The joint PDFs for all IB sizes indicate a strong correlation between the filtered DNS fields and TPIV results, with a correlation coefficient $\rho > 0.97$ in all cases. Note that only the IB = 32 vx and IB = 64 vx JPDFs are included for concision. Additionally, application of the IB = 32 vx TPIV filter was applied to a reacting portion of the flow; the JPDF is shown in Fig. 8(c). There was no observed difference in filter performance of the TPIV filters applied on non-reacting portions of the flow versus reacting portions.

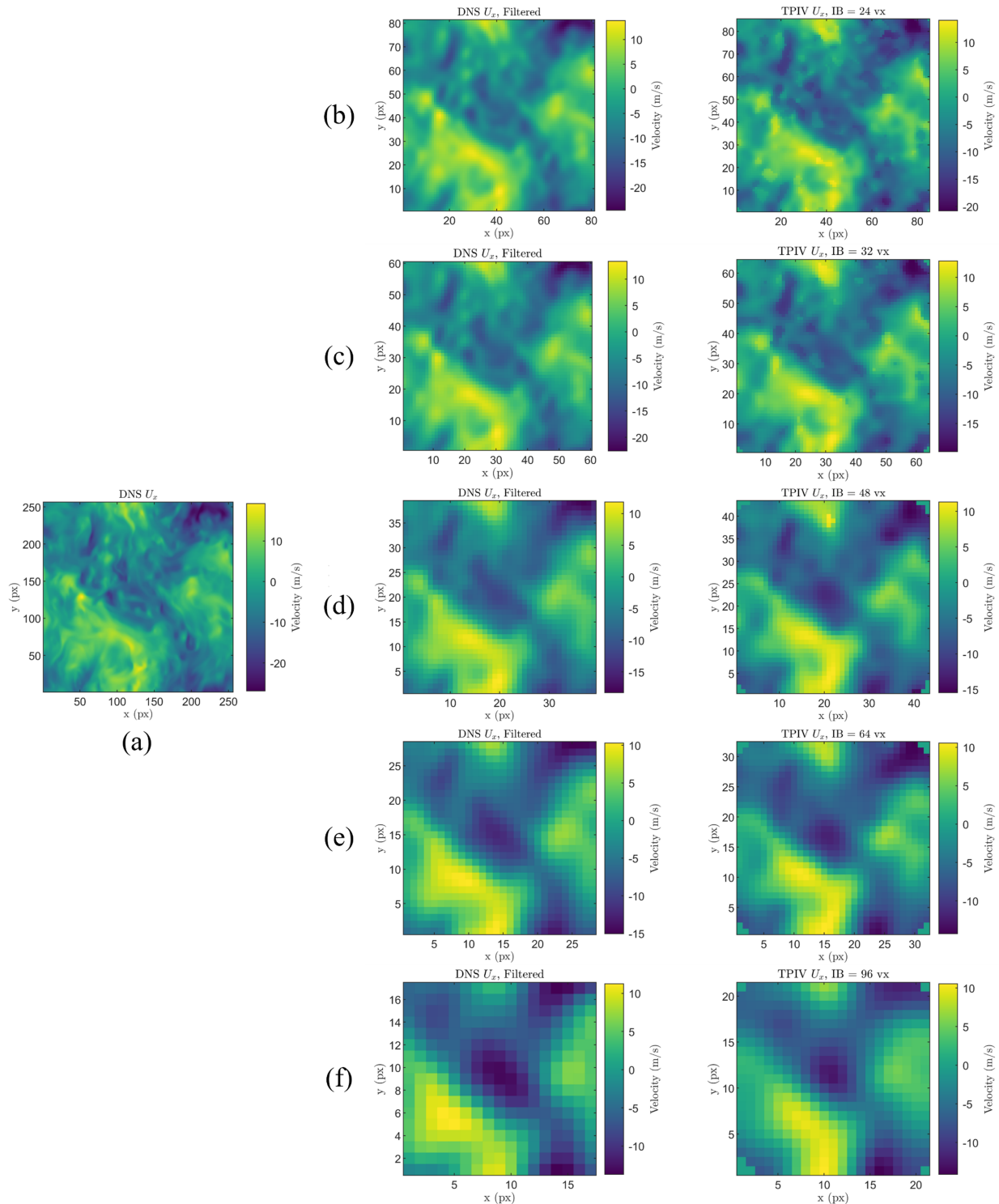


Fig. 7 One slice of the results of applying the TPIV filters on a DNS field. (a) The DNS field. (b) The filtered DNS field using the IB = 24 vx filter and the corresponding TPIV IB = 24 vx output. (c) IB = 32 vx. (d) IB = 48 vx. (e) IB = 64 vx. (f) IB = 96 vx.

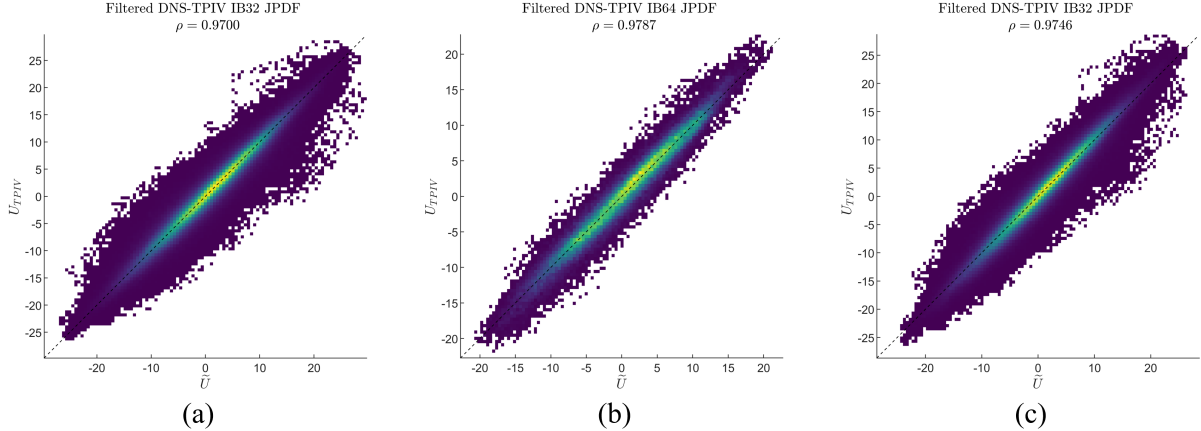


Fig. 8 Joint PDFs between filtered DNS fields and TPIV fields. (a) Non-reacting flow field, IB = 32 vx. (b) Non-reacting flow field, IB = 64 vx. (c) Reacting flow field, IB = 32 vx

IV. Conclusion

This study has presented an analysis of the filter kernel associated with tomographic particle image velocimetry (TPIV). Procedurally-generated step-response velocity fields are used to create synthetic tomograms that are processed by TPIV software. The output TPIV velocity fields are averaged, differentiated, and normalized to acquire the 1D point spread function, also referred to as the 1D intensity profile. Autoconvolution of the 1D intensity profile creates the 3D TPIV convolution kernel. Several other approaches were considered, including Fourier analysis, optimization, and different 3D weighting schemes, but all proved inconclusive. The results indicate that the shape of the TPIV filter kernel is based on a blend of a Mexican-hat wavelet function and a Gaussian profile; the hybrid function is labeled as a "Mexican-hat Gauss". Indeed, the 1D profile of the TPIV filter kernel can be curve-fit onto a superposition of the Mexican-hat and Gaussian functions to a high degree of correlation; the coefficients of the curve-fit function can be used to construct TPIV filter kernels of any interrogation box size, as the filter shape does not vary with IB size. The TPIV filter kernel results were validated by convolving DNS velocity fields with the filter kernel and comparing the output to TPIV velocity fields created by running DNS data through TPIV software. Filtered and TPIV outputs appear extremely similar, with little difference in the smoothing of velocity features and magnitudes; highly correlated JPDFs verify this observation.

It is hoped that the results presented herein can be used to great benefit for anyone working with TPIV measurements, and that the results can be further proven in real-world applications.

Acknowledgments

Special thanks are given to Dr. Askar Kazbekov, whose PhD thesis work provided the motivation for this paper. This research would not have been possible without his guidance and support. Additional acknowledgements are given to Dr. Ryan Darrang and Dr. Peter Hamlington of the University of Colorado, Boulder for providing the DNS data used in this study.

References

- [1] Raffel, M., Willert, C. E., Scarano, F., Kähler, C. J., Wereley, S. T., and Kompenhans, J., *Particle Image Velocimetry*, Springer International Publishing, Cham, 2018. <https://doi.org/10.1007/978-3-319-68852-7>.
- [2] Elsinga, G. E., Scarano, F., Wieneke, B., and van Oudheusden, B. W., "Tomographic particle image velocimetry," *Experiments in Fluids*, Vol. 41, No. 6, 2006, pp. 933–947. <https://doi.org/10.1007/s00348-006-0212-z>.
- [3] Humble, R. A., Elsinga, G. E., Scarano, F., and van Oudheusden, B. W., "Three-dimensional instantaneous structure of a shock wave/turbulent boundary layer interaction," *Journal of Fluid Mechanics*, Vol. 622, 2009, pp. 33–62. <https://doi.org/10.1017/S0022112008005090>.

- [4] Osborne, J. R., Ramji, S. A., Carter, C. D., Peltier, S., Hammack, S., Lee, T., and Steinberg, A. M., “Simultaneous 10 kHz TPIV, OH PLIF, and CH₂O PLIF measurements of turbulent flame structure and dynamics,” *Experiments in Fluids*, Vol. 57, No. 5, 2016, p. 65. <https://doi.org/10.1007/s00348-016-2151-7>.
- [5] Adhikari, D., Gemmell, B. J., Hallberg, M. P., Longmire, E. K., and Buskey, E. J., “Simultaneous measurement of 3D zooplankton trajectories and surrounding fluid velocity field in complex flows,” *Journal of Experimental Biology*, Vol. 218, No. 1, 2015, pp. 3534–3540. <https://doi.org/10.1242/jeb.121707>.
- [6] Meneveau, C., and Katz, J., “Scale-Invariance and Turbulence Models for Large-Eddy Simulation,” *Annual Review of Fluid Mechanics*, Vol. 32, No. 1, 2000, pp. 1–32. <https://doi.org/10.1146/annurev.fluid.32.1.1>.
- [7] O’Brien, J., Urzay, J., Ihme, M., Moin, P., and Saghafian, A., “Subgrid-scale backscatter in reacting and inert supersonic hydrogen-air turbulent mixing layers,” *Journal of Fluid Mechanics*, Vol. 743, 2014, pp. 554–584. <https://doi.org/10.1017/jfm.2014.62>.
- [8] O’Brien, J., Towery, C. A., Hamlington, P. E., Ihme, M., Poludnenko, A. Y., and Urzay, J., “The cross-scale physical-space transfer of kinetic energy in turbulent premixed flames,” *Proc. Combust. Inst.*, Vol. 36, No. 2, 2017, pp. 1967–1975. <https://doi.org/10.1016/j.proci.2016.05.005>.
- [9] Towery, C. A. Z., Poludnenko, A. Y., Urzay, J., OBrien, J., Ihme, M., and Hamlington, P. E., “Spectral kinetic energy transfer in turbulent premixed reacting flows,” *Phys. Rev. E*, Vol. 93, No. 5, 2016. <https://doi.org/10.1103/PhysRevE.93.053115>.
- [10] Kim, J., Bassenne, M., Towery, C. A. Z., Hamlington, P. E., Poludnenko, A. Y., and Urzay, J., “Spatially localized multi-scale energy transfer in turbulent premixed combustion,” *J. Fluid Mech.*, Vol. 848, 2018, pp. 78–116. <https://doi.org/10.1017/jfm.2018.371>.
- [11] Kazbekov, A., Shi, A., Steinberg, A. M., Darragh, R. A., and Hamlington, P. E., “Evaluation of Deconvolution Methods to Estimate Energy Dynamics from Filtered Velocity Measurements,” *AIAA SCITECH 2023 Forum*, American Institute of Aeronautics and Astronautics, Reston, Virginia, 2023. <https://doi.org/10.2514/6.2023-0345>.
- [12] Kazbekov, A., “Inter-Scale Energy Transfer in Turbulent Premixed Combustion,” Ph.D. thesis, Georgia Institute of Technology, 2022. URL <https://hdl.handle.net/1853/70169>.
- [13] Elsinga, G., and Westerweel, J., “The point-spread-function and the spatial resolution of PIV cross-correlation methods,” *9th International Symposium On Particle Image Velocimetry – PIV’11*, Tsukuba, Japan, 2011. URL https://archive.org/download/elsinga-9th-ISPIV-2011/PIV11_Elsinga_DEF.pdf.
- [14] Atkinson, K., *An Introduction to Numerical Analysis*, 2nd ed., John Wiley and Sons, New York, 1991, Chap. 6.
- [15] Darragh, R., Towery, C. A. Z., Meehan, M. A., and Hamlington, P. E., “Lagrangian analysis of enstrophy dynamics in a highly turbulent premixed flame,” *Physics of Fluids*, Vol. 33, No. 5, 2021, p. 055120. <https://doi.org/10.1063/5.0042571>.
- [16] Darragh, R., Towery, C. A., Poludnenko, A. Y., and Hamlington, P. E., “Particle pair dispersion and eddy diffusivity in a high-speed premixed flame,” *Proceedings of the Combustion Institute*, Vol. 38, No. 2, 2021, pp. 2845–2852. <https://doi.org/10.1016/j.proci.2020.06.056>.
- [17] Oppenheim, A. V., and Schafer, R. W., *Discrete-Time Signal Processing*, 2nd ed., Prentice Hall, Upper Saddle River, New Jersey, 1999, Chaps. 8, 9.
- [18] Singh, A., Rawat, A., and Raghuthaman, N., “Mexican Hat Wavelet Transform and Its Applications,” *Methods of Mathematical Modelling and Computation for Complex Systems*, Studies in Systems, Decision and Control, Vol. 373, edited by J. Singh, H. Dutta, D. Kumar, D. Baleanu, and J. Hristov, Springer International Publishing, 2022, pp. 299–317. https://doi.org/10.1007/978-3-030-77169-0_12.
- [19] Westerweel, J., “Digital particle image velocimetry: Theory and application,” Ph.D. thesis, Delft University of Technology, Delft, 6 1993.